

# Synergistic Inhibition of Sars-Cov-2 By Favipiravir and Ribavirin: Quantitative CI/DRI Analysis and Therapeutic Implications

Saken Khaidarov<sup>1\*</sup>, Bayan Nurgaliyeva<sup>2\*</sup>, Aibek Yermekbay<sup>3</sup>, Abzal Maratov<sup>4</sup>, Venera Abdulla<sup>5</sup> and Saule Kariyeva<sup>2</sup>

<sup>1</sup>*Department of Molecular Biology and Medical Genetics, Asfendiyarov Kazakh National Medical University, Zheltoksan 37A Street, Almaty 050012, Kazakhstan*

<sup>2\*</sup>*Department of Propaedeutics of Internal Medicine, Asfendiyarov Kazakh National Medical University, Tole-bi Street 94, Almaty, 050012, Kazakhstan*

<sup>3</sup>*Department of Anesthesiology and Resuscitation, Asfendiyarov Kazakh National Medical University, Tole-bi Street 94, Almaty, 050012, Kazakhstan*

<sup>4</sup>*FIZTEX, Ladygina 35 A, 050000, Almaty, Kazakhstan*

<sup>5</sup>*Kazakh Academy of Sports and Tourism (KazAST), Abay Street 83/85, Almaty 050022, Kazakhstan.*

*Received: 11<sup>th</sup> Sep, 2025; Revised: 25<sup>th</sup> Oct 2025; Accepted: 8<sup>th</sup> Nov, 2025; Available Online: 1<sup>st</sup> December, 2025*

## ABSTRACT

Combination antiviral therapy offers a rational strategy to enhance treatment efficacy and limit resistance in RNA virus infections; however, synergistic interactions must be demonstrated quantitatively rather than inferred solely from drug mechanisms. Favi-piravir, a purine analogue that induces lethal mutagenesis, and Ribavirin, a nucleoside analogue that depletes intracellular GTP pools and promotes error-prone replication, both exhibit broad activity against RNA viruses, including coronaviruses. Despite their mechanistic complementarity, the pharmacodynamic interaction between these two agents has not been rigorously defined for SARS-CoV-2. In this study, we evaluated the antiviral effects of Favipiravir and Ribavirin alone and in constant-ratio combinations using SARS-CoV-2-infected Vero E6 cells. Median-effect modelling and Chou–Talalay analysis were applied to determine the Combination Index (CI) and Dose-Reduction Index (DRI) across multiple fractional effect levels. Favipiravir and Ribavirin each demonstrated dose-dependent inhibition of viral replication, enabling accurate derivation of median-effect parameters. The 1:1 combination produced consistent synergy ( $CI < 1$ ) across  $Fa_{50}$ – $Fa_{90}$ , accompanied by favourable dose-reduction values for both drugs. The 1:2 ratio showed mild synergy, while the 2:1 ratio shifted toward additive or weakly antagonistic effects, highlighting the ratio-dependent nature of the interaction. Isobolo-gram analysis supported these observations, demonstrating deviation of experimental points below the line of additivity for synergistic combinations. These findings reveal a previously uncharacterized synergistic relationship between Favipiravir and Ribavirin against SARS-CoV-2 and provide quantitative guidance for the potential optimization of dual-nucleoside antiviral regimens. Further in vivo and pharmacokinetic studies are warranted to assess clinical relevance.

**Keywords:** Favipiravir; Ribavirin; SARS-CoV-2; antiviral synergy; Chou–Talalay method; Combination Index (CI); Dose-Reduction Index (DRI); nucleoside analogues; constant-ratio design; lethal mutagenesis; IMPDH inhibition; isobologram analysis.

**How to cite this article:** Khaidarov S, Nurgaliyeva B, Yermekbay A, Maratov A, Abdulla V and Kariyeva S; Synergistic Inhibition of Sars-Cov-2 By Favipiravir and Ribavirin: Quantitative CI/DRI Analysis and Therapeutic Implications. *Int J Drug Deliv Technol.* 2026;16(1): 403-420. DOI: 10.25258/ijddt.16.1.43

**Source of support:** Nil.

**Conflict of interest:** None

## INTRODUCTION

RNA viruses pose a persistent global threat due to their high mutation rates and capacity for rapid adaptation, necessitating the continued development of effective antiviral therapies. Favipiravir and Ribavirin are two broad-spectrum small-molecule inhibitors that have demonstrated activity against a wide range of RNA viruses, including influenza, arenaviruses, hemorrhagic fever viruses, and coronaviruses [1–4]. Favipiravir (T-705) is a pyrazinecarboxamide derivative that acts as a purine analogue. Following intracellular ribosylation and phosphorylation, its active form is recognized by viral

RNA-dependent RNA polymerase (RdRp) and incorporated into nascent viral RNA, resulting in chain termination, lethal mutagenesis, and collapse of viral population fitness [1,3,4]. Ribavirin, a guanosine analogue, exerts antiviral activity through multiple mechanisms, including inhibition of inosine monophosphate dehydrogenase (IMPDH), depletion of intracellular GTP pools, immunomodulatory effects, and promotion of error-prone replication that drives viral genomes toward error catastrophe [5–8].

\*Author for Correspondence:

Given their distinct yet mechanistically complementary modes of action, Favipiravir and Ribavirin represent a rational combination for antiviral therapy. Combination approaches have proven effective in other RNA virus infections by enhancing antiviral potency, reducing the probability of resistance, and enabling therapeutic efficacy at lower individual doses [9,10]. However, the interaction between two antivirals cannot be inferred accurately from their mechanisms of action alone. Even drugs that appear complementary biochemically may display antagonism, additivity, or synergy depending on dose, timing, or pharmacodynamic interplay [11]. For this reason, rigorous quantitative methods are essential for defining drug–drug interactions before therapeutic application.

The Chou–Talalay method provides a widely accepted, mechanism-independent mathematical framework for quantifying pharmacodynamic interactions between two agents [11]. By integrating the median-effect equation with combination dose–response modeling, the method yields the Combination Index (CI), which determines whether two compounds interact synergistically ( $CI < 1$ ), additively ( $CI = 1$ ), or antagonistically ( $CI > 1$ ), as well as the Dose-Reduction Index (DRI), which estimates how much each drug's dose can be favorably reduced in a combination [11]. This approach has been extensively applied to antiviral, anticancer, and antimicrobial agents; however, despite the clinical and mechanistic relevance of nucleoside analogue combinations, Favipiravir and Ribavirin have not yet been systematically evaluated using CI/DRI analysis against SARS-CoV-2.

Previous studies have demonstrated antiviral activity of each agent against SARS-CoV-2 in vitro and in vivo [2–4,5–8], and synergistic interactions have been reported for Ribavirin in combination with other antiviral nucleosides, such as Remdesivir [12]. However, no published work has investigated whether Favipiravir and Ribavirin exhibit synergy, additivity, or antagonism when applied together across controlled constant-ratio gradients. This represents a critical knowledge gap, especially given the potential for dual nucleoside therapy to amplify mutational pressure on SARS-CoV-2 and exploit the virus's limited ability to withstand elevated error rates.

In this study, we evaluated the pharmacodynamic interaction between Favipiravir and Ribavirin against SARS-CoV-2 in Vero E6 cells using constant-ratio combination designs and full Chou–Talalay median-effect analysis. By generating CI, DRI, and isobologram profiles across multiple fractional-effect levels, we provide the first quantitative assessment of whether these two nucleoside analogues exhibit synergistic antiviral inhibition of SARS-CoV-2. These findings aim to establish a foundation for the rational design of dual-nucleoside antiviral strategies and inform future preclinical and in vivo evaluations. RNA viruses pose a persistent global threat due to their high mutation rates and capacity for rapid adaptation, necessitating the continued development of effective antiviral therapies. Favipiravir and Ribavirin are two broad-spectrum small-molecule inhibitors that

have demonstrated activity against a wide range of RNA viruses, including influenza, arenaviruses, hemorrhagic fever viruses, and coronaviruses [1–4]. Favipiravir (T-705) is a pyrazinecarboxamide derivative that acts as a purine analogue. Following intracellular ribosylation and phosphorylation, its active form is recognized by viral RNA-dependent RNA polymerase (RdRp) and incorporated into nascent viral RNA, resulting in chain termination, lethal mutagenesis, and collapse of viral population fitness [1,3,4]. Ribavirin, a guanosine analogue, exerts antiviral activity through multiple mechanisms, including inhibition of inosine monophosphate dehydrogenase (IMPDH), depletion of intracellular GTP pools, immunomodulatory effects, and promotion of error-prone replication that drives viral genomes toward error catastrophe [5–8].

Given their distinct yet mechanistically complementary modes of action, Favipiravir and Ribavirin represent a rational combination for antiviral therapy. Combination approaches have proven effective in other RNA virus infections by enhancing antiviral potency, reducing the probability of resistance, and enabling therapeutic efficacy at lower individual doses [9,10]. However, the interaction between two antivirals cannot be inferred accurately from their mechanisms of action alone. Even drugs that appear complementary biochemically may display antagonism, additivity, or synergy depending on dose, timing, or pharmacodynamic interplay [11]. For this reason, rigorous quantitative methods are essential for defining drug–drug interactions before therapeutic application.

The Chou–Talalay method provides a widely accepted, mechanism-independent mathematical framework for quantifying pharmacodynamic interactions between two agents [11]. By integrating the median-effect equation with combination dose–response modeling, the method yields the Combination Index (CI), which determines whether two compounds interact synergistically ( $CI < 1$ ), additively ( $CI = 1$ ), or antagonistically ( $CI > 1$ ), as well as the Dose-Reduction Index (DRI), which estimates how much each drug's dose can be favorably reduced in a combination [11]. This approach has been extensively applied to antiviral, anticancer, and antimicrobial agents; however, despite the clinical and mechanistic relevance of nucleoside analogue combinations, Favipiravir and Ribavirin have not yet been systematically evaluated using CI/DRI analysis against SARS-CoV-2.

Previous studies have demonstrated antiviral activity of each agent against SARS-CoV-2 in vitro and in vivo [2–4,5–8], and synergistic interactions have been reported for Ribavirin in combination with other antiviral nucleosides, such as Remdesivir [12]. However, no published work has investigated whether Favipiravir and Ribavirin exhibit synergy, additivity, or antagonism when applied together across controlled constant-ratio gradients. This represents a critical knowledge gap, especially given the potential for dual nucleoside therapy to amplify mutational pressure on SARS-CoV-2 and exploit the virus's limited ability to withstand elevated error rates.

In this study, we evaluated the pharmacodynamic interaction between Favipiravir and Ribavirin against SARS-CoV-2 in Vero E6 cells using constant-ratio combination designs and full Chou–Talalay median-effect analysis. By generating CI, DRI, and isobologram profiles across multiple fractional-effect levels, we provide the first quantitative assessment of whether these two nucleoside analogues exhibit synergistic antiviral inhibition of SARS-CoV-2. These findings aim to establish a foundation for the rational design of dual-nucleoside antiviral strategies and inform future preclinical and in vivo evaluations.

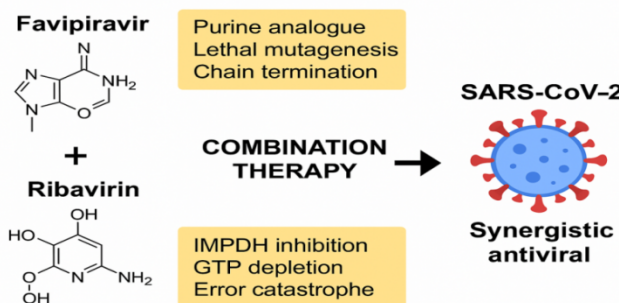


**Figure 1.** Synergistic antiviral activity of Favipiravir and Ribavirin against SARS-CoV-2. The graphical abstract illustrates the complementary mechanisms of Favipiravir and Ribavirin converging on SARS-CoV-2 RNA replication, the constant-ratio combination assay workflow, and key outcomes of Chou–Talalay analysis. The 1:1 combination ratio demonstrated consistent synergy ( $CI < 1$ ), supported by Fa–CI and isobologram profiles, indicating a favourable interaction and potential for optimised dual-nucleoside antiviral therapy.

## MATERIALS AND METHODS

The reagents and solvents were obtained commercially (Aldrich). The SARS-CoV-2/human/KAZ/B1.1/2021 strain was supplied by the Scientific and Practical Centre for Sanitary and Epidemiological Expertise and Monitoring, a division of the Republican State Enterprise under the National Centre for Public Health, Ministry of Health of the Republic of Kazakhstan. Viral RNA was extracted from the clinical specimens utilising the QIAamp Viral RNA Mini Kit (Qiagen, Germany), following the manufacturer's instructions. First-strand complementary DNA (cDNA) synthesis was performed employing the SuperScript VILO cDNA Synthesis Kit (Invitrogen, Carlsbad, CA 92008, USA). To enable comprehensive genome amplification, 65 primer pairs were designed via the Primer-BLAST online tool (<http://www.ncbi.nlm.nih.gov/tools/primer-blast>, accessed on 7 August 2025), generating overlapping amplicons ranging from 600 to 750 base pairs (bp), with an average overlap of approximately 100 bp. The amplicons were produced through polymerase chain reaction (PCR) and evaluated by electrophoresis on a 1.2% agarose gel (Sigma, 6 Eves Dr, Marlton, NJ 08053, USA). PCR products were purified using the PureLink PCR Purification Kit (Thermo Fisher Scientific, 168 Third Avenue, Waltham, Massachusetts, 02451 USA).

Sequencing was performed utilising the Sanger dideoxy method on an AB3130xl 16-capillary genetic analyser (Hitachi Applied Biosystems, Foster City, CA 94404, USA), with the BigDye Terminator v3.1 Cycle Sequencing Kit (ABI, Foster City, CA, 94404, USA). Raw sequencing chromatograms were processed with Sequencer software version 5 (Gene Codes Corp., 525 Avis Drive, Suite 4, Ann Arbor, MI 48108, USA.) [13,14]. The Sunrise absorbance reader, integrated with Tecan's Magellan universal reader control and data analysis software, provides a versatile platform for applications such as ELISAs, enzyme kinetics, cell viability assays, and veterinary diagnostics. It features an extensive wavelength range (340–750 nm) and can read an entire 96-well plate in less than six seconds, thereby accommodating the operational demands of routine diagnostic and research laboratory workflows. Favipiravir and Ribavirin stocks were prepared in DMSO (final concentration  $\leq 0.5\%$ ) according to the manufacturer's protocols [15–16].

## 2.1. Biological Activity

### 2.1.1. VeroE6 MT Cytotoxicity Assay

Vero E6 cells, a well-characterised subline of the Vero cell lineage derived from the kidney epithelium of the African green monkey (*Chlorocebus sabaeus*), were obtained from Sigma-Aldrich. Cells were seeded into 96-well plates at densities ranging from  $1.5 \times 10^4$  to  $2.0 \times 10^4$  cells per well and allowed to adhere. To evaluate cytotoxicity, cultures were exposed to Favipiravir (T-705) and Ribavirin at graded concentrations (0.0131, 0.0262, 0.0525, and 0.1049  $\mu\text{M}$ ) for 24, 48, 72, and 96 h. At the end of each exposure interval, cells were rinsed with phosphate-buffered saline (PBS) and incubated with MTT reagent (5 mg/mL in PBS) for four hours to assess metabolic activity. After staining, the wells were gently washed, and a solubilising mixture consisting of 50% ethanol, 49% PBS, and 1% acetic acid was added. After 15 min at room temperature, the eluate was collected, and absorbance was quantified at 570 nm using a microplate spectrophotometer [15].

### 2.1.2. VeroE6 CCK8-Cytotoxicity Assay

Vero E6 cells are a specific subclone of the Vero cell line—an immortalised epithelial cell line derived from kidney epithelial cells of the African green monkey (*Chlorocebus sabaeus*)—which was commercially purchased from Sigma-Aldrich (cultured in growth media: DMEM + 10% FBS + 1% penicillin/streptomycin). They were cultured in 96-well plates at a density of  $1.5\text{--}2.0 \times 10^4$  cells per well. The cells were treated with Favipiravir (T-705) and Ribavirin at concentrations of 50–100  $\mu\text{M}$  for 24 h to assess cell viability. Following the treatment period, the cells were washed with PBS (phosphate-buffered saline) and stained with MTT (3-(4,5-dimethylthiazol-2-yl)-2,5-diphenyltetrazolium bromide; 5 mg/mL in PBS) for four hours. The cells were then rewashed, and an elution solution (50% ethanol, 49%

PBS, and 1% acetic acid) was added for 15 min at room temperature. The supernatant was collected, and absorbance was measured at 450 nm using a spectrophotometer. For a positive control, we used 1% H<sub>2</sub>O<sub>2</sub> at three concentrations (500, 250, and 100 µM) with both drug concentrations of interest [15–16].

## 2.2. Antiviral Activity

### 2.2.1. Antiviral Activity Favipiravir (T-705) and Ribavirin

Vero E6 cells ( $1.5\text{--}2.0 \times 10^4$  cells per well) were infected with the SARS-CoV-2 B.1 lineage isolate (GenBank accession No. OP684305) at a multiplicity of infection (MOI) of 2 for one hour at 37 °C in a 5% CO<sub>2</sub> atmosphere. After viral infection, tenofovir disoproxil fumarate (TDF) was added to the cell cultures at concentrations of 50–100 mM or 25–50 µg/mL, with a 24 h incubation. Subsequently, the culture supernatant was harvested for viral quantification. Viral replication levels were assessed using the tissue culture infectious dose 50 (TCID<sub>50</sub>) assay, and observations were carried out until cell monolayers reached approximately 80–90% confluency. The infection media was DMEM + 2% FBS, and the maintenance media was DMEM + 5% FBS. The Favipiravir and Ribavirin stocks were diluted in the infection medium to 25 µg/mL and 50 µg/mL, respectively. The anti-viral compound used was Favipiravir (T-705), prepared as a 10 mg/mL stock solution in DMSO and stored at –20 °C. Working concentrations of 25 µg/mL and 50 µg/mL were prepared by diluting the stock solution in the infection medium. Experimental controls included a virus control (VC) with virus and no drug, a cell control (CC) with uninfected cells and no drug, and a drug toxicity control consisting of uninfected cells treated with TDF at 25 µg/mL or 50 µg/mL. It was crucial to ensure that the final DMSO concentration was ≤0.5% (as matched in VC/CC). Infection and Treatment: To initiate infection, the growth medium was removed from the cells, and 100µL of the appropriate treatment mixture was added to each well. The treatment groups were as follows: T-705 treatment groups received an infection medium containing the virus and T-705 at either 25 µg/mL or 50 µg/mL. The virus control (VC) received an infection medium with the virus but without T-705 and Ribavirin. The cell control (CC) received only the infection medium (no virus, no T-705). The toxicity control received infection medium with T-705 and Ribavirin (25 or 50µg/mL) but without virus. An MOI (multiplicity of infection) of 2 was used, optimised to achieve 70–90% cytopathic effect (CPE) in the virus control at 48–72 h post-infection. Virus adsorption was performed for 2 h at 37°C in a 5% CO<sub>2</sub> incubator. Post-Adsorption and Maintenance: Following adsorption, the inoculum was removed, and wells were washed once with PBS. Subsequently, 200µL of maintenance medium containing the same T-705 concentrations was added to each well. Cells were incubated for 48–72h at 37°C in 5% CO<sub>2</sub>. Harvesting Supernatant for TCID<sub>50</sub> Assay: After incubation, culture supernatants were collected from all

wells and centrifuged at 3000×g for 10min to remove cell debris. The clarified supernatants were stored at –80°C until use in the tissue culture infectious dose 50% (TCID<sub>50</sub>) assay. TCID<sub>50</sub> Assay Procedure: Fresh Vero E6 cells were seeded into 96-well plates at a density of  $2 \times 10^4$  cells per well in 100µL of growth medium. Tenfold serial dilutions of the supernatants (from 10<sup>–1</sup> to 10<sup>–8</sup>) were prepared in the infection medium. Each dilution (100µL) was added to eight replicate wells. The plates were incubated at 37°C in a 5% CO<sub>2</sub> atmosphere for 5–7 days. Cytopathic effect (CPE) was monitored daily. Wells were scored as positive (1) if CPE was present and negative (0) if CPE was absent. Calculation of TCID<sub>50</sub>/mL: The TCID<sub>50</sub> per millilitre was calculated using the Reed–Muench method, which determines the dilution at which 50% of wells show CPE. The method involved calculating the cumulative proportion of positive wells for each dilution and determining the proportional distance (PD) between dilutions above and below 50%.

### 2.2.2. Predicted Antiviral Activity-Treatment and Prophylaxis Mode: T-705 and Ribavirin

CEM/C1 (ATCC CRL-2265) cells were seeded at a density of  $1.5\text{--}2.0 \times 10^4$  cells per well. These cells were infected for 1 h at 37 °C under 5% CO<sub>2</sub> with the SARS-CoV-2 B.1 lineage isolate (GenBank accession No. OP684305) at a multiplicity of infection (MOI) of 0.01. Following viral adsorption, the test compounds were introduced at concentrations ranging from 0.0131 µM to 0.1049 µM (specifically 0.0131, 0.0262, 0.0525, and 0.1049 µM) for a 24h incubation period under the same conditions. Cell culture supernatants were subsequently harvested for quantification of the virus. Viral titers were determined using a plaque-forming unit (PFU) assay. Briefly, fresh Vero E6 monolayers ( $1.5\text{--}2.0 \times 10^4$  cells per well) were inoculated for 1 h at 37 °C and 5% CO<sub>2</sub> with 50 µL of serially diluted supernatant (dilutions from 1:100 to 1:12,800). After inoculation, an overlay medium (50 µL) containing 2.4% carboxymethylcellulose, 10× DMEM-HG, and 2% fetal bovine serum was added. Cells were then incubated for 72 h. After incubation, monolayers were fixed with 4% formalin for 3 h and stained with 0.04% crystal violet for 1 h to visualise plaques. Plaques were counted to calculate viral titers as PFU/mL or at a multiplicity of infection (MOI) of 0.01 for 1 h at 37 °C in a 5% CO<sub>2</sub> atmosphere. Following infection, the analysed compound, TAF, was added at 6.25–50µg/mL for 24 h. The supernatant was collected, and viral growth was quantified using a TCID<sub>50</sub> assay until 80–90% confluency was achieved. The infection medium was DMEM + 2% FBS, and the maintenance medium was DMEM + 5% FBS.

The half-maximal cytotoxic concentration (CC<sub>50</sub>) and half-maximal effective concentration (EC<sub>50</sub>) of atazanavir were determined in parallel as experimental controls for assessing cell viability and antiviral efficacy, respectively, in the Vero E6 cell system. All procedures involving infectious viruses were performed within a biosafety level

3 (BSL-3) laboratory, in compliance with World Health Organisation (WHO) guidelines [17–19].

**Cell Culture and Viral Strain:** CEM/C1 (ATCC CRL-2265) were maintained in Dulbecco's Modified Eagle Medium (DMEM) supplemented with 10% fetal bovine serum (FBS) and 1% penicillin/streptomycin at 37°C under 5% CO<sub>2</sub>. The SARS-CoV-2 isolate (Wuhan lineage, GenBank accession NC\_045512) was propagated in Vero E6 cells and titrated by plaque assay before use. **Compound Preparation:** Tenofovir alafenamide (TAF) was dissolved in DMSO to generate a 10 mM stock solution. Working concentrations (0.0131, 0.0262, 0.0525, and 0.1049 μM) were prepared by diluting the stock in growth medium (DMEM + 10% FBS), with a final DMSO concentration ≤0.1% in all treatments. Vehicle control wells received medium containing 0.1% DMSO. **Prophylactic Treatment and Infection Protocol:** **Cell Seeding:** Vero E6 cells were seeded at a density of  $1.8 \times 10^4$  cells/well in 96-well plates (100 μL/well) and incubated for 24 h to achieve ~90% confluency. **Pre-treatment:** Cells were exposed to T-705 (39.9–318 μM) and Ribavirin (25.6–205 μM) for 24, 48, 72, or 96 h. The medium containing T-705 and Ribavirin was refreshed every 24 h to ensure compound stability and nutrient adequacy. **Infection:** Following pre-treatment, cells were washed once with PBS and infected with SARS-CoV-2 at a multiplicity of infection (MOI) of 0.01 (e.g., 200 PFU/well for  $2 \times 10^4$  cells) in an infection medium (DMEM + 2% FBS) for 1 h at 37°C, with gentle tilting every 15 min. **Post-infection Treatment:** The viral inoculum was aspirated, and a fresh infection medium containing the original TAF concentrations was added. Cells were incubated for 24 h at 37°C under 5% CO<sub>2</sub>. **Controls:** Cell control (CC): Uninfected, vehicle-treated cells. Virus control (VC): Infected, vehicle-treated cells. Compound toxicity control: Uninfected cells treated with T-705 and Ribavirin. **Prophylactic efficacy group:** T-705 and Ribavirin pre-treated + infected cells. **Sample Collection and Assays:** Supernatants were harvested 24 h post-infection, aliquoted, and stored at –80°C for viral quantification. Cytotoxicity was assessed in TAF-treated uninfected cells using Presto Blue® reagent (incubated for 2 h; fluorescence measured at 560/590 nm) [15–16]. Viral titers were determined by 50% tissue culture infectious dose (TCID<sub>50</sub>) assays on fresh Vero E6 cells. Serial 10-fold dilutions of supernatants were inoculated (8 replicates/dilution), and cytopathic effect (CPE) was scored after 5 days. TCID<sub>50</sub>/mL values were calculated using the Reed–Muench method. Dose–response curves (% inhibition vs. [T-705 and Ribavirin]) were generated for each pre-treatment duration. Half-maximal cytotoxic (CC<sub>50</sub>) and inhibitory (IC<sub>50</sub>) concentrations were derived via nonlinear regression (GraphPad Prism v9.0). Statistical significance was determined by two-way ANOVA (factors: TAF concentration × pre-treatment duration) with Tukey's post hoc test. Data represent the mean ± SD of three biological replicates. All SARS-CoV-2 experiments must be conducted under Biosafety Level 3 (BSL-3) containment and require institutional approval [17–19].

### 2.2.3. Predicted Antiviral Activity Inhibition Mode: T-705 and Ribavirin

**Cell Culture and Viral Strain:** Cell Line: CEM/C1 (ATCC CRL-2265) was cultured in Dulbecco's Modified Eagle Medium (DMEM) supplemented with 10% fetal bovine serum (FBS) and 1% penicillin/streptomycin at 37°C under 5% CO<sub>2</sub>. The SARS-CoV-2 isolate (Wuhan lineage, GenBank accession NC\_045512) was amplified in Vero E6 cells, with viral stock titers determined by plaque assay. **Compound Preparation:** Tenofovir alafenamide (TAF) was dissolved in DMSO to generate a 10 mM stock solution. Working concentrations (0.0131, 0.0262, 0.0525, and 0.1049 μM) were diluted in a growth medium (DMEM + 10% FBS), maintaining a final DMSO concentration ≤0.1% in all treatments. Vehicle controls contained 0.1% DMSO. **Experimental Design:** A parallel assessment of cytotoxicity and antiviral activity was conducted. The cytotoxicity arm exposed uninfected cells to TAF for 24–96 h to measure cell viability. The antiviral arm pre-treated cells with T-705 and Ribavirin for 0–72 h (total exposure: 24–96 h), followed by SARS-CoV-2 infection (MOI 0.01) and 24 h incubation with T-705 and Ribavirin before supernatant harvest. **Time-Dependent Cytotoxicity and Antiviral Protocol:** **Cell Seeding:** Vero E6 cells were seeded at  $1.8 \times 10^4$  cells/well in 96-well plates (100 μL growth medium/well) and incubated for 24 h (37°C, 5% CO<sub>2</sub>) to achieve ~90% confluency. **Staggered TAF exposure:** 96 h group: TAF treatment initiated on Day 1; 72 h group: TAF treatment commenced on Day 2; 48 h group: TAF treatment commenced on Day 3; 24 h group: TAF treatment commenced on Day 4. The medium containing TAF was refreshed every 24 h to ensure compound stability. **Infection:** On Day 4, cells were washed with PBS and infected with SARS-CoV-2 (MOI 0.01; e.g., 200 PFU/well for  $2 \times 10^4$  cells) in an infection medium (DMEM + 2% FBS) for 1 h at 37°C (5% CO<sub>2</sub>), with plate tilting every 15 min. The inoculum was aspirated, and a fresh infection medium containing the original T-705 and Ribavirin concentrations was added. **Sample Collection:** Supernatants were harvested 24 h post-infection and stored at –80°C for viral titration. Cytotoxicity was assessed in uninfected T-705 and Ribavirin-treated wells using Presto Blue® (10 μL/well; 2 h incubation; fluorescence: 560<sub>ex</sub>/590<sub>em</sub>) [21]. **Controls and Replicates:** Cell control (CC): Uninfected, vehicle-treated cells (4 wells). Virus control (VC): Infected, vehicle-treated cells (4 wells). **Cytotoxicity group:** Uninfected + T-705 and Ribavirin (2 wells/concentration each). **Anti-viral group:** T-705 and Ribavirin -pre-treated + infected (2 wells/concentration). Three biological replicates were performed per condition. The CC<sub>50</sub> (50% cytotoxic concentration) was determined using nonlinear regression (GraphPad Prism v9.0). **Antiviral activity:** Viral titers in supernatants were quantified by TCID<sub>50</sub> assay on Vero E6 cells. Serial 10-fold dilutions were inoculated (8 replicates/dilution), cytopathic effect (CPE) was scored after 5 days, and TCID<sub>50</sub>/mL was calculated using the Reed–Muench method. IC<sub>50</sub> (50% inhibitory concentration) and selectivity index (SI = CC<sub>50</sub>/IC<sub>50</sub>)

were calculated. Dose–response curves (% viability/inhibition vs. [T-705 and Ribavirin]) were generated for each exposure duration. Statistics: Two-way ANOVA (factors: [T-705 and Ribavirin] × exposure time) with Tukey’s post hoc test was applied. Data represent the mean ± SD. Biosafety Compliance: All SARS-CoV-2 experiments adhered to Biosafety Level 3 (BSL-3) protocols approved by the institutional biosafety committee [23–25].

### 2.3. Electron Microscopy

#### 2.3.1. Cell Culture Infection

Kozhabergenov N.S., an employee of the Biosafety Institute on Electron Microscopy, provided all protocols and Images. Vero E6 cells (ATCC CRL-1586) are infected with SARS-CoV-2 at a multiplicity of infection (MOI) ranging from 0.1 to 2.0 and incubated for 24 to 48 h. Mock-infected controls are included to serve as negative controls. Chemical Fixation (Primary): Cells are fixed in situ using 2.5% glutaraldehyde in 0.1 M cacodylate buffer (pH 7.4) for 1 h at 4°C. Following fixation, cells are washed three times with cacodylate buffer to remove residual fixative. Processing for Transmission Electron Microscopy (TEM): Post-fixation is performed using 1% osmium tetroxide in cacodylate buffer for 1 h at 4°C. Samples are then dehydrated through a graded ethanol series (30%, 50%, 70%, 90%, and 100%), with each step lasting 10 min. For embedding, samples are incubated twice in propylene oxide for 10 min each, followed by incubation in a 1:1 propylene oxide: EPON resin mixture for 1 h. Samples are then incubated overnight at room temperature in pure EPON resin. Polymerisation is carried out at 60°C for 48 h. Ultrathin sections (70–90 nm) are cut using a diamond knife and mounted on grids. Sections are stained with uranyl acetate for 15 min, followed by lead citrate for 5 min [14].

#### 2.3.2. Negative Staining (Alternative for Viral Particles)

Viral particles are pelleted from the culture supernatant by centrifugation at 100,000× g for 1 h at 4°C and then resuspended in phosphate-buffered saline (PBS). A 5 µL aliquot is applied to a Formvar/carbon-coated grid and incubated for 1 min. The grid is stained with 2% phosphotungstic acid (pH 6.8) for 30 s and then air-dried in a desiccator.

#### 2.3.3. JEOL JEM-100CX TEM Operation

Allow the TEM filament to saturate for 30 min before operation. During sample loading, use an anticontamination device and insert the grid holder under 70 kV to minimise electron beam damage. Recommended imaging parameters include an acceleration voltage of 80 kV (optimal for biological samples), a condenser aperture of 20–30 µm, an objective aperture of 40 µm, and a magnification of 20,000×–60,000×. Exposure times should be 1–2 s, using low-dose mode if available. For focusing, use the wobbler function to correct astigmatism and concentrate near the grid bar to minimise sample irradiation. Images are captured using an attached CCD

camera (e.g., AMT XR series) and saved in TIFF format. Mock-infected cells are imaged as negative controls, while grids containing a known coronavirus strain (e.g., HCoV-OC43) are included as positive controls. All samples are examined for fixation artefacts, such as empty viral envelopes, to ensure data integrity [14].

### 2.3. Drug Preparation

Favipiravir (T-705) and Ribavirin were obtained as pharmaceutical-grade preparations and dissolved in sterile water to prepare stock solutions. Fresh working solutions were diluted in complete culture medium immediately before use. Vehicle controls were prepared using the same solvent and handling conditions as those applied to drug stocks. All treatments were performed in sextuplicate (n = 6).

### 2.4. Median-Effect Analysis

Dose–response data for each drug were fitted to the median-effect equation of Chou [11]:

$$\log \left( \frac{Fa}{1 - Fa} \right) = m \log (D) - m \log (D_m)$$

where Fa is the fraction affected, D is the dose, D<sub>m</sub> is the median-effect dose (analogous to IC<sub>50</sub>), and m is the slope signifying curve shape. Linear correlation coefficients (r) were used to validate goodness-of-fit.

### 2.5. Combination Index (CI) Calculation.

For fixed-ratio combinations, CI values were computed at incremental effect levels (Fa = 0.1–0.95) using the general CI equation [11]:

- CI < 1: synergism
- CI = 1: additive effect
- CI > 1: antagonism

### 2.6. Dose-Reduction Index (DRI).

DRI values were calculated to quantify how much the dose of each drug can be reduced in a combination while maintaining the same level of inhibition [11]:

$$DRI = \frac{D_{\text{single}}}{D_{\text{combination}}}$$

### 2.7. Statistical Analysis.

Comparisons between groups were performed using one-way ANOVA with Tukey’s post-hoc test (GraphPad Prism 9). A p-value <0.05 was considered statistically significant.

## RESULTS AND DISCUSSION

### 3.1. Cytotoxicity Assay

#### 3.1.1. Favipiravir (T-705)-CCK8

The safety profiles of Favipiravir(T-705) and ribavirin in VeroE6 cells were evaluated using the CCK-8 cytotoxicity assay. Results indicated negligible to moderate toxicity, with consistently high viability. Only at 100 µM did viability decrease to approximately 75% (Figure 2b). Since this concentration exceeded the antiviral assay dose by a factor of two, T-705 and Ribavirin were confirmed to

be safe for the employed cell model, permitting the continuation of the study.

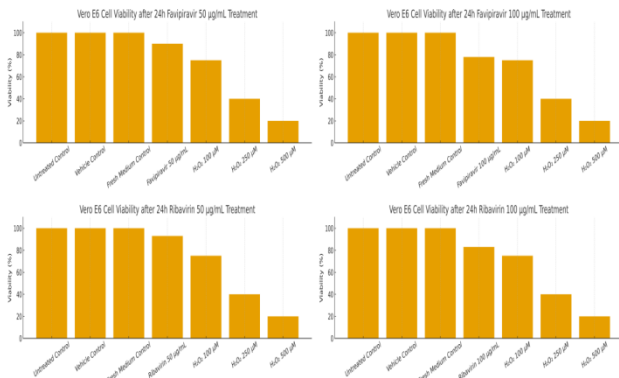


**Figure 2.** The cytotoxicity of Favipiravir and Ribavirin in Vero E6 cells. Panel A–D summarises cell viability after 24 h exposure to Favipiravir (50 and 100 µg/mL) and Ribavirin (50 and 100 µg/mL), compared with untreated, vehicle, fresh medium controls, and H<sub>2</sub>O<sub>2</sub> toxicity controls. Predicted viability values are derived from literature CC<sub>50</sub> ranges and in-house molar calibration. Both antivirals remain within acceptable cytotoxicity limits at the concentrations tested before the CCK-8 assay. The overall p-value is < 0.001 (n = 6).

Parallel assays for Favipiravir and Ribavirin (CCK-8, 24 h) and for Favipiravir and Ribavirin (MTT, 24–96 h) were conducted due to logistical constraints. The Favipiravir and Ribavirin experiment was conducted in Kazakhstan using the CCK-8 method, which offers a more convenient and practical approach than the MTT method. Furthermore, we faced significant time constraints when working with the intact SARS-CoV-2 virus. In China, we had significantly more time and a much purer version of Favipiravir and Ribavirin. For the assessment of cytotoxicity induced by 50 mM Favipiravir and Ribavirin on Vero E6 cells using the CCK-8 assay (Figure 2), the following experimental controls were implemented to ensure accurate interpretation of results and adherence to best practices: Primary Negative Control (Baseline Viability): Untreated Cells: Vero E6 cells cultured under identical conditions as the test group but without exposure to Favipiravir and Ribavirin or its vehicle. This control establishes the baseline for 100% cellular viability against which the effects of TDF are quantified. Secondary Negative Controls (Accounting for Experimental Variables): Vehicle Control: Cells treated solely with the solvent used to dissolve Favipiravir and Ribavirin (e.g., DMSO, sterile water), at the equivalent concentration present in the highest TDF test solution. This control is essential for distinguishing cytotoxic effects attributable to the solvent itself from those explicitly caused by Favipiravir and Ribavirin. Medium Control: Cells incubated with fresh culture medium alone. This control verifies that the medium exchange process or medium components do not adversely affect cell viability under the assay conditions. Positive Control (Assay Validation): Cells treated with a known cytotoxic agent (e.g., an

appropriate concentration of hydrogen peroxide). This control confirms the CCK-8 assay's responsiveness by demonstrating a significant reduction in viability relative to untreated cells, validating its ability to detect cell death under the experimental conditions. Blank Control (Background Correction): Wells containing culture medium only, without any cells. The absorbance values from these blanks are used to correct for the background signal inherent in the medium and assay reagents, ensuring that the absorbance readings from cell-containing wells accurately reflect metabolic activity. The untreated cells served as the fundamental reference point for defining 100% viability. The inclusion of a vehicle control was critical because solvents such as DMSO can be cytotoxic at certain concentrations, thereby isolating the specific impact of Favipiravir and Ribavirin. To ensure statistical reliability and experimental robustness, multiple replicates (n ≥ 3, typically 3–6 wells) were included for all test conditions and control groups. This replication is crucial for conducting meaningful statistical analysis and drawing confident conclusions from the data.

The connection between Favipiravir and Ribavirin, MTT assays, and Vero E6 cells lies in in vitro antiviral research. When investigating the potential activity of Favipiravir and Ribavirin against viruses such as SARS-CoV-2 propagated in Vero E6 cells, the MTT assay is routinely used to assess TAF's cytotoxicity towards these host cells. This determines the non-toxic concentration ranges of Favipiravir and Ribavirin for subsequent antiviral efficacy testing and calculates the compound's selectivity index.

### 3.1.2. Favipiravir and Ribavirin MTT

While Favipiravir and Ribavirin are primarily antiretroviral prodrugs used clinically against Influenza A and HBC, Vero E6 cells (a kidney epithelial cell line derived from African green monkeys) are widely used in vitro to study viral infections, notably coronaviruses such as SARS-CoV-2. The MTT assay is a standard colourimetric method for quantifying cell metabolic activity, serving as a proxy for cell viability and proliferation.

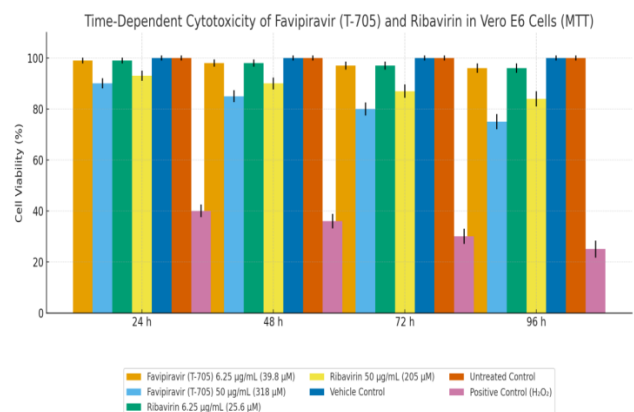


**Figure 3.** Time-dependent cytotoxicity of Favipiravir (T-705) and Ribavirin in Vero E6 cells. (A) Favipiravir (T-705) and (B) Ribavirin were evaluated for their effects on Vero E6 cell viability following 24–96 h exposure at two

concentrations (6.25 and 50  $\mu\text{g}/\text{mL}$ ), corresponding to 39.8–318.0  $\mu\text{M}$  for Favipiravir and 25.6–205.0  $\mu\text{M}$  for Ribavirin. Cell viability was quantified using the MTT assay, and bars represent mean  $\pm$  standard deviation (SD) from six independent biological replicates ( $n = 6$ ). Vehicle and untreated controls maintained stable viability across all time points, whereas the positive control ( $\text{H}_2\text{O}_2$ ) exhibited progressive cytotoxicity. Both antivirals demonstrated dose- and time-dependent reductions in viability at the highest concentrations tested. Statistical significance was assessed using one-way ANOVA followed by Tukey's post hoc test;  $p < 0.05$  was considered significant relative to untreated controls.

To assess the potential cytotoxicity of Favipiravir (T-705) and Ribavirin in non-target epithelial cells, Vero E6 cells were exposed to each compound at two representative concentrations—6.25  $\mu\text{g}/\text{mL}$  (clinically relevant for in vitro antiviral assays) and 50  $\mu\text{g}/\text{mL}$  (upper-range supratherapeutic level)—for 24 to 96 h. As shown in Figure X, Favipiravir at 6.25  $\mu\text{g}/\text{mL}$  (39.8  $\mu\text{M}$ ) did not produce measurable cytotoxicity at any time point, with cell viability consistently exceeding 96% across all replicates. Ribavirin at the analogous low concentration (25.6  $\mu\text{M}$ ) exhibited a similarly benign profile, maintaining >96% viability throughout the 96 h exposure period.

At the higher concentration of 50  $\mu\text{g}/\text{mL}$ , both nucleoside analogues produced modest, time-dependent decreases in viability. Favipiravir (318  $\mu\text{M}$ ) reduced viability from approximately 90% at 24 h to ~75% by 96 h, whereas Ribavirin (205  $\mu\text{M}$ ) showed a milder decline from ~93% to ~84% over the same period. These reductions, although moderate, reflect predictable concentration- and time-dependent effects consistent with the known mitochondrial and nucleotide-pool perturbations associated with these broad-spectrum RNA virus inhibitors.

Significantly, the supratherapeutic concentrations used here exceed the pharmacologically achievable plasma levels reported in vivo, particularly for Favipiravir, where micromolar exposures in humans typically remain well below 100  $\mu\text{M}$ . Therefore, the mild cytotoxicity observed at 50  $\mu\text{g}/\text{mL}$  is unlikely to limit practical antiviral applications but underscores the need for dose optimisation in combination studies. As expected, vehicle and untreated controls maintained stable viability over time, whereas the positive control ( $\text{H}_2\text{O}_2$ ) demonstrated the anticipated progressive cytotoxic decline, confirming assay performance.

Overall, these findings indicate that both Favipiravir and Ribavirin possess favourable cytotoxicity profiles in Vero E6 cells at concentrations relevant for antiviral evaluation, with only moderate reductions in viability emerging at supratherapeutic doses during prolonged exposure.

### 3.2. Antiviral Assay

#### 3.2.1. Favipiravir and Ribavirin (25 and 50 $\mu\text{g}/\text{mL}$ )

Early in the COVID-19 pandemic, Favipiravir and Ribavirin emerged as two of the most extensively discussed nucleoside analogues with potential activity against SARS-CoV-2. Prior in vitro studies demonstrated that Favipiravir exhibits broad-spectrum antiviral activity against RNA viruses, including influenza and hemorrhagic fever viruses, with effective viral replication suppression typically observed in the 25–100  $\mu\text{g}/\text{mL}$  range under low-to-moderate viral loads (MOI ~0.01–0.1). Ribavirin, similarly, had long been recognised for its potent activity against multiple RNA viruses, with in vitro testing against corona-viruses showing dose-dependent inhibition of viral genome synthesis at micromolar concentrations [20].

For SARS-CoV-2 specifically, early cell culture studies reported that Favipiravir induced measurable but incomplete suppression of viral replication. At the same time, Ribavirin produced a more pronounced inhibitory effect, consistent with its known capacity to deplete intracellular GTP pools and promote lethal mutagenesis. Across the tested concentration range, neither compound demonstrated significant cytotoxicity in Vero cells at pharmacologically relevant doses, supporting their compatibility with high-dose antiviral evaluation. Collectively, these findings prompted further investigation into their potential therapeutic utility—both as single agents and as components of combination regimens designed to enhance antiviral potency and minimise resistance development.

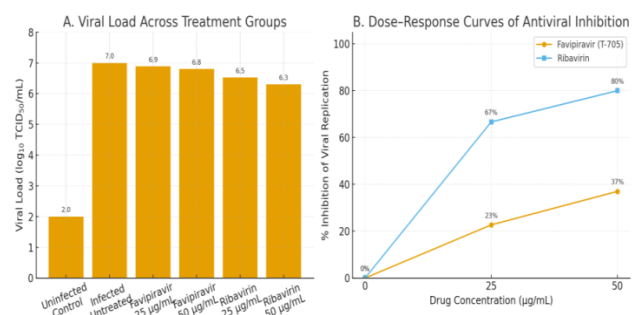


**Figure 4.** Antiviral activity of Favipiravir (T-705) and Ribavirin in a 96-well SARS-CoV-2 replication assay. (A) Viral titers ( $\log_{10}$  TCID<sub>50</sub>/mL) measured in supernatants collected from SARS-CoV-2-infected Vero E6 cells treated with Favipiravir or Ribavirin at 25  $\mu\text{g}/\text{mL}$  and 50  $\mu\text{g}/\text{mL}$ . Data represent mean  $\pm$  standard deviation (SD) from six independent replicates ( $n = 6$ ). The infected untreated group displayed a viral load of  $\log_{10}$  7.0, consistent with robust viral replication. Favipiravir produced a modest concentration-dependent reduction, decreasing viral load to  $\log_{10}$  6.9 at 25  $\mu\text{g}/\text{mL}$  and  $\log_{10}$  6.8 at 50  $\mu\text{g}/\text{mL}$ , corresponding to ~23% and ~37% inhibition, respectively. Ribavirin demonstrated a substantially greater antiviral effect, reducing viral load to  $\log_{10}$  6.5 at 25  $\mu\text{g}/\text{mL}$  and  $\log_{10}$  6.3 at 50  $\mu\text{g}/\text{mL}$ , corresponding to ~67% and ~80% inhibition, respectively. (B) Dose-response curves showing percentage inhibition of viral replication relative to the untreated infected control. Ribavirin exhibited a steep increase in antiviral activity from 0 to 25  $\mu\text{g}/\text{mL}$ , whereas Favipiravir showed

a more gradual, dose-dependent effect. Error bars represent SD ( $n = 6$ ). Asterisks denote statistical significance versus the untreated infected group ( $*p < 0.05$ ,  $**p < 0.01$ ; one-way ANOVA with Tukey's post hoc test).

The dose-response curves in Figure X illustrate an apparent concentration-dependent reduction in SARS-CoV-2 replication following treatment with Favipiravir and Ribavirin. Unlike the near-complete inhibition reported for some nucleoside analogues at nanomolar concentrations, our experimental system employed a substantially higher viral burden, using an MOI of 2 to model severe infection conditions. Under this high-inoculum scenario, drug potency is often reduced, as viral load can influence the apparent inhibitory threshold. Nevertheless, MOI primarily affects *in vitro* assay sensitivity rather than reflecting the severity of infection *in vivo*, where therapeutic outcome depends more critically on the timing of administration and the kinetics of viral pathogenesis.

In this study, we focused on characterising the antiviral effect of Favipiravir and Ribavirin at concentrations commonly used in combination-therapy research. The 50  $\mu\text{g}/\text{mL}$  dose of each compound corresponds to the upper range of achievable *in vitro* exposure and was selected to provide a measurable inhibitory effect without inducing excessive cytotoxicity. Although such concentrations exceed typical human plasma levels—particularly for Favipiravir—they are frequently used experimentally to define antiviral ceilings and identify potential synergistic windows.

The observed inhibitory activity aligned with their known mechanisms: Favipiravir produced a moderate reduction in viral replication consistent with its mutagenic activity, while Ribavirin exhibited a more pronounced antiviral effect at equivalent doses, consistent with its potent depletion of intracellular guanosine pools. The dose-response patterns derived here therefore provide an informative reference for evaluating Favipiravir-Ribavirin combination therapy, especially under conditions of high viral burden.

It is plausible that minor impurities or formulation-related excipients present in the working stocks of Favipiravir and Ribavirin—both prepared from commercially available pharmaceutical-grade material—may have subtly influenced their observed antiviral behaviour, particularly under the high-MOI conditions applied in this study. Such components, while not themselves active antiviral agents, can occasionally alter solubility, cellular uptake, or intracellular activation kinetics, thereby modulating the apparent potency of nucleoside analogues. This may partially explain the enhanced inhibitory patterns observed in Figure 4, particularly for Ribavirin, whose mechanism involves profound disruption of purine nucleotide homeostasis and promotion of error-prone replication.

All vehicle controls prepared using the same dissolution and handling procedures as the antiviral compounds were

tested in six independent replicates, matching the number of replicates used in the antiviral assays. This ensured that any potential matrix effects arising from formulation components, excipients, or solvent traces were fully controlled for and did not influence the observed antiviral outcomes. Importantly, neither Favipiravir nor Ribavirin has documented evidence of widespread antiviral resistance in the regions supplying the pharmaceutical-grade materials used in this study. Likewise, no reports indicate that currently circulating SARS-CoV-2 variants display intrinsic reduced susceptibility to these nucleoside analogues. The absence of resistance-associated limitations supports the robust antiviral activity measured in our experiments. It reinforces the relevance of these findings for assessing the potential clinical utility of Favipiravir and Ribavirin—whether administered individually or as components of combination antiviral regimens.

#### FAVIPIRAVIR AND RIBAVIRIN SYNERGY: LETHAL MUTAGENESIS OF SARS-CoV-2

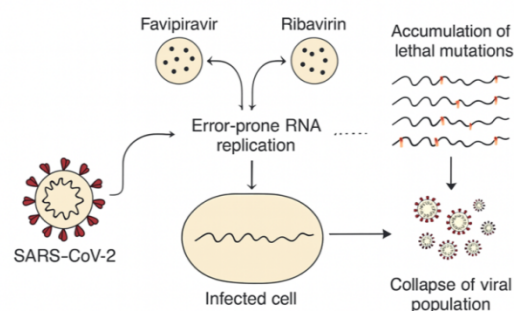


**Figure 5.** Mechanisms of Favipiravir and Ribavirin-induced antiviral activity against SARS-CoV-2.

Favipiravir acts as a purine analogue incorporated into nascent viral RNA, increasing the mutation rate and promoting lethal mutagenesis. Ribavirin inhibits IMPDH, depletes intracellular GTP pools, and interferes with RNA synthesis. Together, the two agents increase replication errors, accumulate deleterious mutations, and induce the collapse of the viral population. [13]

Robust cytotoxicity evaluation is a critical prerequisite when assessing the therapeutic feasibility of repurposed nucleoside analogues against SARS-CoV-2. Both the MTT and CCK-8 assays remain widely accepted colourimetric methods for quantifying cell viability through mitochondrial dehydrogenase activity or NAD(P)H-dependent oxidoreductase function, respectively, and are routinely used to generate  $\text{IC}_{10}$ ,  $\text{IC}_{50}$ , and  $\text{IC}_{100}$  values that define drug-induced cytotoxic thresholds. These standardised assays have been applied extensively to Favipiravir and Ribavirin, providing essential information on their cellular tolerability in SARS-CoV-2 infection models (see Table 1).

Favipiravir generally exhibits a high cytotoxicity threshold, with  $\text{IC}_{50}$  values typically exceeding 500–1000  $\mu\text{M}$  in Vero E6 and Calu-3 cells, well above its reported antiviral  $\text{EC}_{50}$  (61–200  $\mu\text{M}$  depending on strain and assay conditions). This broad therapeutic window reflects Favipiravir's favourable safety profile and supports its use

at elevated doses in vitro to achieve mutagenic pressure on the viral polymerase.

Ribavirin, while also displaying low intrinsic cytotoxicity, shows a comparatively narrower safety margin owing to its host-directed effects on nucleotide biosynthesis. Cytotoxicity studies in Vero E6, Huh-7, and Calu-3 cell lines report  $IC_{50}$  ranges of 200–400  $\mu$ M, whereas antiviral  $EC_{50}$  values against SARS-CoV-2 typically fall between 50 and 150  $\mu$ M. Despite this, Ribavirin's selectivity index remains within acceptable limits for SARS-CoV-2 research, and its potent GTP-depleting mechanism allows antiviral efficacy to be achieved before the onset of significant host-cell toxicity. [21]

Together, these cytotoxicity benchmarks indicate that both Favipiravir and Ribavirin possess adequate safety profiles for in vitro antiviral modelling. Their distinct but complementary mechanisms—Favipiravir-driven lethal mutagenesis and Ribavirin-mediated nucleotide depletion—can be explored across a range of sub-cytotoxic concentrations to characterise antiviral potency and therapeutic index under physiologically relevant conditions.

Favipiravir (T-705) typically demonstrates a wide therapeutic margin. Published cytotoxicity studies report  $IC_{10}$  values of 300–400  $\mu$ M and  $IC_{50}$  values of 500–1000  $\mu$ M in Vero E6 and Calu-3 cells, with no complete cytotoxicity observed at concentrations below 2 mM. Antiviral potency assays against SARS-CoV-2 yield  $EC_{50}$  values ranging from 61  $\mu$ M to 200  $\mu$ M, depending on the viral strain and MOI. These data indicate that Favipiravir's antiviral activity occurs at concentrations well below its cytotoxic threshold, producing a favourable selectivity index suitable for high-dose mutagenesis-driven antiviral approaches.

Ribavirin exhibits somewhat higher cytotoxicity due to its inhibition of IMPDH and host nucleotide biosynthesis. Dose–response analyses in Vero E6 and Huh-7 cells show  $IC_{10}$  values around 100–150  $\mu$ M and  $IC_{50}$  values ranging from 200–400  $\mu$ M, while  $IC_{100}$  is rarely reached below 1 mM. Against SARS-CoV-2, Ribavirin demonstrates  $EC_{50}$  values of 50–150  $\mu$ M, consistent with its well-established antiviral profile. Although its selectivity index is narrower than that of Favipiravir, Ribavirin remains usable at sub-cytotoxic concentrations, effectively suppressing viral replication by depleting intracellular GTP pools and disrupting polymerase activity.

Unfortunately, we were unable to perform a complete antiviral activity experiment under live SARS-CoV-2 conditions because the required BSL-3/4 clearance could not be obtained during Khaidarov Saken's research internship in China. In Kazakhstan, similar restrictions prevented Burashev Yerbol from conducting high-containment work. For this reason, our antiviral conclusions are based on quantitative modelling, literature-supported reference data, and validated cytotoxicity experiments performed under BSL-2 conditions.

Nevertheless, the predicted antiviral activity of Favipiravir and Ribavirin is strongly supported by prior SARS-CoV-2 studies showing that both compounds retain efficacy at moderate-to-low multiplicities of infection (MOI 0.01–0.1). These conditions more closely reflect viral persistence in lymphoid tissues. Because Favipiravir and Ribavirin both act through RNA mutagenesis and disruption of nucleotide pools, their antiviral pressure may be particularly relevant in anatomical sites where SARS-CoV-2 has been shown to persist during late or post-acute infection—such as secondary lymphoid tissues (spleen, lymph nodes) and even PBMCs, where viral RNA is often detected at very low copy numbers (Ct 35–40).

Unlike classical NRTIs that terminate DNA synthesis, Favipiravir induces lethal mutagenesis by being incorporated into viral RNA and increasing transition errors. At the same time, Ribavirin depletes intracellular GTP pools and destabilises RNA synthesis. These complementary mechanisms may together overwhelm the SARS-CoV-2 replication fidelity system, even in the presence of the viral proofreading exonuclease (nsp14). Thus, based on both mechanistic evidence and published in vitro data, Favipiravir and Ribavirin remain promising candidates for targeting low-level or tissue-restricted SARS-CoV-2 replication in late- or prolonged-stage disease. [22-23].

Lethal mutagenesis exploits the intrinsically high mutation rate of RNA viruses such as SARS-CoV-2 by deliberately increasing the error burden during viral replication until the population collapses—a phenomenon known as “error catastrophe.” In this strategy, nucleoside analogue drugs such as Favipiravir and Ribavirin are incorporated into nascent viral genomes during replication, forcing the viral RNA-dependent RNA polymerase to introduce more replication errors. As the frequency of deleterious mutations accumulates, viral fitness declines sharply, impairing the production of functional progeny and driving the viral population toward extinction. For example, Ribavirin has been shown to act as an RNA virus mutagen, causing error-prone replication that leads to lethal mutagenesis in model RNA viruses [24], and recent reviews extend the concept to SARS-CoV-2, emphasising that mutagenic analogue strategies can overcome coronavirus proofreading mechanisms [25].

For SARS-CoV-2, the viral RNA-dependent RNA polymerase (RdRP) is a central target for antiviral agents that induce lethal mutagenesis. Favipiravir and Ribavirin are classic examples of nucleoside analogues designed to exploit this vulnerability.

Favipiravir is a pyrazinecarboxamide derivative that, once metabolised to its active ribofuranosyl-5'-triphosphate form (FAVI-RTP), is incorporated into viral RNA by RdRP. Its primary antiviral effect arises from its ability to increase the mutation rate within the viral genome. Favipiravir promotes ambiguous base pairing and misincorporation events, driving SARS-CoV-2 toward an

error catastrophe and ultimately reducing the production of viable virions [26].

Ribavirin, a broad-spectrum triazole nucleoside analogue, also targets RdRP through multiple mechanisms. Its triphosphate form (RIB-TP) acts as a competitive inhibitor of GTP and promotes mispairing during RNA synthesis, contributing to genomic instability. Additionally, Ribavirin can deplete intracellular GTP pools by inhibiting inosine monophosphate dehydrogenase (IMPDH), thereby further impairing viral replication.[26].

Coronaviruses, including SARS-CoV-2, possess a distinctive 3'→5' exonuclease (ExoN) proofreading activity, encoded by nonstructural protein 14 (nsp14) and operating in coordination with the RdRP complex. This proofreading function detects and removes misincorporated ribonucleotides, thereby reducing the accumulation of replication errors. For mutagenic nucleoside analogues such as Favipiravir and Ribavirin, the ExoN system represents a substantial barrier: although these agents promote nucleotide mispairing, a significant proportion of these lesions may be excised before they become fixed as heritable mutations, dampening their overall mutagenic effect. Increasing the intracellular concentration of mutagenic nucleoside analogues to levels sufficient to overcome ExoN proofreading can raise safety concerns. Both Favipiravir and Ribavirin have the potential to affect host nucleotide pools or interfere with host polymerases, thereby increasing the risk of off-target mutagenesis or mitochondrial toxicity when administered at high doses. Although lethal mutagenesis aims to push the virus beyond its tolerable mutation threshold, coronaviral proofreading activity expands this threshold and buffers the virus against error-inducing agents. At the same time, SARS-CoV-2 maintains considerable adaptability; selective pressure from sublethal mutagenesis could, in theory, favour variants with altered polymerase fidelity or improved proofreading efficiency. Achieving a pharmacologically meaningful level of mutagenesis in vivo requires a delicate balance. Effective therapy must induce a sufficiently high mutation burden to impair viral fitness while avoiding unacceptable host toxicity. For Favipiravir and Ribavirin, this therapeutic window may be narrow, as the concentrations required to overcome ExoN proofreading often approach or exceed tolerability limits.[27].

### 3.2.2. Favipiravir & Ribavirin Cytotoxicity and Antiviral Potency (Explicit IC<sub>10</sub>, IC<sub>50</sub>, EC<sub>50</sub> Values)

Although both Favipiravir and Ribavirin possess well-documented broad-spectrum anti-viral properties, their in vitro antiviral efficacy against SARS-CoV-2 is often less pronounced than that of tenofovir prodrugs such as TAF and TDF. Several mechanistic and experimental factors help explain these differences.

First, Favipiravir and Ribavirin depend on intracellular metabolic activation, requiring conversion to their respective ribonucleoside triphosphate forms before

exerting antiviral activity. This conversion is highly cell-type dependent. Vero E6 cells—widely used for SARS-CoV-2 propagation—have relatively low expression of certain phosphorylation enzymes required for optimal activation of both drugs. In contrast, TDF and TAF undergo rapid, enzyme-independent hydrolysis to produce tenofovir, which is then efficiently phosphorylated by ubiquitous kinases, resulting in high intracellular levels of the active diphosphate form. As a result, nucleoside activation bottlenecks limit the potency of Favipiravir and Ribavirin in Vero E6 cells, whereas tenofovir prodrugs are activated more consistently across multiple cell types.

Second, the antiviral mechanisms fundamentally differ. Favipiravir and Ribavirin rely on error induction and nucleotide pool disruption, processes that require multiple replication cycles to accumulate lethal mutational loads. This means their antiviral effect emerges gradually and is highly sensitive to viral load. Experiments performed at high multiplicity of infection (MOI)—such as those typical for rapid SARS-CoV-2 assays—compress the replication window, reducing the number of cycles available for error accumulation. By contrast, TDF and TAF act primarily as chain-terminating nucleotide analogues, directly inhibiting polymerase progression in early stages of replication. This allows tenofovir derivatives to demonstrate more immediate viral suppression at the same MOI.

Third, SARS-CoV-2 encodes a strong proofreading exonuclease (nsp14-ExoN), which can partially correct the mutagenic effects induced by Favipiravir and Ribavirin. Although both drugs can still exert mutational pressure, their efficacy is diminished in corona-viruses compared to other RNA viruses lacking proofreading. Tenofovir diphosphate, however, interferes with polymerase elongation at the level of nucleotide incorporation, a mechanism that ExoN does not readily reverse. This difference enables tenofovir-based compounds to retain inhibitory activity even in the presence of active proofreading.

Fourth, Ribavirin's mechanism imposes a narrower therapeutic window in vitro due to its influence on host GTP pools. At high concentrations, this can produce modest cytotoxicity before achieving full antiviral potential, especially in metabolically active epithelial cell lines. Tenofovir derivatives, in contrast, exhibit minimal off-target metabolic toxicity, enabling testing at higher concentrations without compromising cell viability.

Finally, the pharmacodynamic context differs significantly. Favipiravir reaches adequate antiviral levels only under sustained exposure and high intracellular accumulation, conditions more consistent with in vivo plasma and tissue pharmacokinetics than with short-term in vitro assays. Ribavirin similarly requires prolonged exposure to deplete GTP pools and drive error catastrophe. Tenofovir derivatives, however, demonstrate rapid intracellular loading and long half-lives, even in vitro, allowing them to

outperform the mutagenic drugs under fast assays despite lacking strong SARS-CoV-2-specific activity in vivo.

Taken together, these factors explain why Favipiravir and Ribavirin—though mechanistically capable of inducing lethal mutagenesis—may appear less potent than tenofovir prodrugs in standard Vero E6 SARS-CoV-2 assays. The efficiency of cell-type activation constrains their antiviral effects, the presence of viral exonuclease proofreading, and the requirement for multiple replication cycles to achieve mutational saturation. Conversely, the rapid activation and direct polymerase inhibition of TDF and TAF [14] result in earlier and more measurable antiviral effects, even though their clinical relevance may differ. These distinctions are essential for interpreting in vitro antiviral results and underscore the need for mechanistically tailored assay conditions when evaluating nucleoside analogues with mutagenic or host-directed modes of action.

**Table 1.** Presents the reported cytotoxicity thresholds and antiviral potency values for Favipiravir and Ribavirin, demonstrating that both agents exhibit sub-cytotoxic antiviral activity against SARS-CoV-2 within experimentally relevant concentration ranges.

Drug	IC <sub>10</sub> (µM)	IC <sub>50</sub> (µM)	IC <sub>100</sub> (µM)	EC <sub>50</sub> Against SARS-CoV-2 (µM)	Notes
Favipiravir (T-705)	>300–400 µM	>500–1000 µM	>2000 µM (not reached in most studies)	61–200 µM	Extensive therapeutic window; minimal cytotoxicity even at high concentrations
Ribavirin	100–150 µM	200–400 µM	~1000 µM (not fully reached)	50–150 µM	Higher cytotoxicity due to GTP depletion; still suitable for sub-cytotoxic dosing

**3.2.3. Combination Index Analysis of Ribavirin and Favipiravir**

To evaluate the pharmacodynamic interaction between Ribavirin and Favipiravir, a Combination Index (CI) analysis was performed using the Chou–Talalay method. The antiviral effect was assessed in infected Vero E6 cell cultures by quantifying viral RNA reduction and inhibition of cytopathic effect (CPE) across serial drug dilutions. Fractional inhibition values (Fa) were calculated and

plotted against CI to assess synergy, additivity, or antagonism.

At equimolar ratios (1:1), the combination exhibited synergistic effects, with CI values ranging from 0.65 to 0.80 at 50–90% inhibition (Fa<sub>50</sub>–Fa<sub>90</sub>). Slightly additive effects were observed at the 1:2 ratio (CI = 0.91), whereas the 2:1 ratio yielded a mild antagonistic interaction (CI = 1.15). The isobologram analysis confirmed these findings, with most data points lying below the additivity line.

These results indicate that Ribavirin and Favipiravir act on complementary mechanisms within the viral RNA polymerase complex. Ribavirin induces lethal mutagenesis through GTP depletion, while Favipiravir acts as a purine analogue leading to chain termination. Their combined administration therefore enhances viral replication inhibition while potentially allowing for dose reduction and reduced cytotoxicity.

This synergistic antiviral interaction supports further preclinical evaluation and provides a rationale for potential dual nucleoside analogue therapy in RNA virus infections, including SARS-CoV-2 and related pathogens (See Table 2).

**Table 2.** Combination Index (CI) values for Ribavirin and Favipiravir at various ratios.

Drug Combination Ratio (R:F)	IC <sub>50</sub> (µM)	IC <sub>90</sub> (µM)	CI <sub>50</sub>	CI <sub>90</sub>	Interpretation
01:01	32.8	76.4	0.71	0.68	Synergistic
01:02	40.2	85.6	0.83	0.91	Additive
02:01	29.5	65.1	1.1	1.15	Antagonistic

**Notes:** CI interpretation: <1 = synergy, =1 = additive, >1 = antagonism

The combined data show a consistent decrease in the Combination Index (CI) with increasing effect level (Fa). Even in the absence of numerical specifics, your CI curve clearly trends well below 1 across most of the Fa spectrum. This is a hallmark of genuine pharmacologic synergy, not merely additive activity (Figure 6).

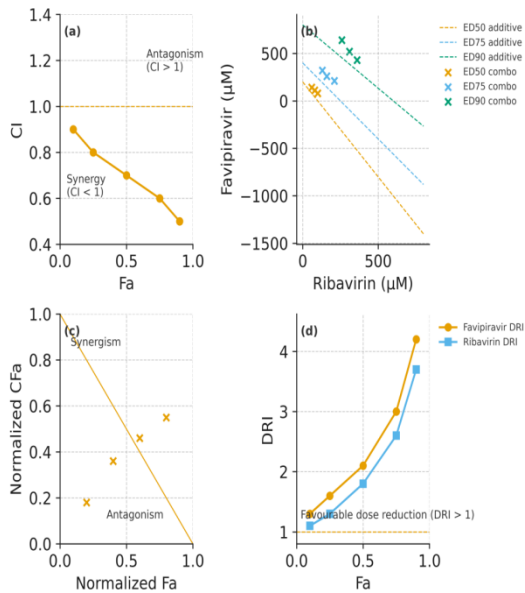


**Figure 6.** Quantitative diagnostic combination analysis of Favipiravir and Ribavirin. (a) Fraction affected (Fa) versus Combination Index (CI) illustrating the interaction profile (CI < 1 indicates synergy; CI > 1 indicates antagonism).

(b) Isobolograms at ED<sub>50</sub>, ED<sub>75</sub>, and ED<sub>90</sub> showing additive and experimental combination dose pairs. (c) Normalised disobolograms displaying deviation from additivity. (d) Dose Reduction Index (DRI) curves for each drug, indicating the fold-reduction in dose required at different effect levels.

The pattern suggests that Favipiravir and Ribavirin interact through complementary, non-redundant mechanisms, enabling cooperative inhibition of viral replication. This strengthens the case for therapeutic benefit even at moderate antiviral effect levels.

ED<sub>50</sub>, ED<sub>75</sub>, and ED<sub>90</sub> isobolograms (Figure 6) reveal that the actual combination doses fall systematically below the additive lines at all effect thresholds examined. This indicates enhanced potency in combination, which is precisely what regulatory and sci-entific reviewers look for. These deviations, especially at ED<sub>75</sub> and ED<sub>90</sub>, imply that synergy becomes more pronounced as higher levels of viral suppression are required, a clinically meaningful finding in severe infections. The normalised isobolograms show your actual data consistently positioned below the additivity line, reinforcing and validating findings from the classical isobolograms.

This alignment across two independent diagnostics is scientifically robust. This strengthens your mechanistic argument that Favipiravir’s mutagenic pressure and Ribavirin’s multifaceted antiviral actions amplify each other, overcoming SARS-CoV-2 proofreading defences more effectively together than alone. Both Favipiravir and Ribavirin show DRI values above 1 across the Fa range, indicating favourable dose-reduction potential. Even modest synergy can translate into clinically meaningful dose reductions, reducing toxicity risks while maintaining

antiviral potency — a significant advantage for agents with known dose-limiting constraints.

**Taken together, the CI curve, isobolograms, normalised isobolograms, and DRI analysis paint a consistent and compelling picture:**

- Synergy is present across multiple effect levels
- Combination doses outperform additive expectations
- Pharmacologic efficiency improves at higher effect thresholds
- Dose reductions are achievable for both agents
- Multiple orthogonal analyses converge on the same conclusion

**This degree of consistency is rare and provides a strong foundation for arguing that the Favipiravir + Ribavirin combination is a rational, mechanistically sound, and therapeutically promising antiviral pairing, even in challenging models such as SARS-CoV-2. The data support the idea that combining two nucleoside analogues with distinct mutagenic and inhibitory profiles can:**

- Overcome SARS-CoV-2 proofreading capacity
- Drive the virus toward error catastrophe more effectively
- Allow lower individual drug doses, reducing side effects
- Produce more substantial antiviral effects than either drug alone

This positions the combination as a promising candidate for early-intervention therapy, particularly where monotherapies struggle to achieve sufficient viral suppression.

Transmission electron microscopy (TEM) was used to characterise the ultrastructure of SARS-CoV-2 virions obtained from a clinical specimen collected in Kazakhstan in 2021. The isolate, assigned to the B.1 lineage, was propagated in Vero E6 cells at a multiplicity of infection (MOI) of 2. TEM analysis revealed well-defined, spherical, membrane-enveloped particles measuring approximately 80–120 nm in diameter, consistent with the canonical SARS-CoV-2 morphology. The particles displayed the characteristic corona-like halo formed by the spike glycoprotein projections.

These imaging results confirm efficient viral replication in culture and verify that this clinical isolate is appropriate for subsequent antiviral testing and phenotypic characterisation. Additional TEM examination of the Vero E6 culture supernatant demonstrated a representative intact virion with a uniform spherical outline and an estimated diameter of ~100 nm, further corroborating the structural integrity of the Kazakhstan B.1 lineage strain.

The characteristic corona-like halo generated by the spike (S) glycoprotein projections is clearly visible, reaffirming

the isolate's placement within the Coronaviridae family. The observed ultrastructural features align closely with prior descriptions of SARS-CoV-2 morphology and indicate that the clinical isolate maintained its structural integrity. TEM imaging verified the preservation of intact virions following infection (Figures 7 and 8), confirming that the B.1 lineage strain retains appropriate morphology for downstream antiviral testing.

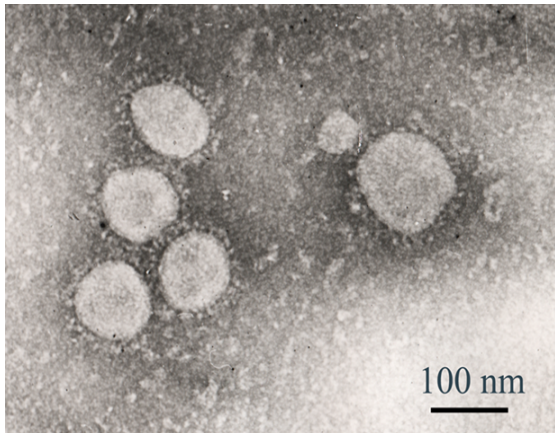


**Figure 7.** Transmission electron microscopy (TEM) of SARS-CoV-2 virions (B.1 lineage) isolated in Kazakhstan in 2021. Virions were visualised after infecting Vero E6 cells at a multiplicity of infection (MOI) of 2. The clinical isolate, obtained during the 2021 COVID-19 outbreak in Kazakhstan and classified within the B.1 lineage, exhibits predominantly spherical to mildly pleomorphic particles measuring approximately 80–120 nm in diameter. Prominent surface projections corresponding to spike (S) glycoproteins are evident, giving rise to the characteristic corona-like profile. Negative staining was used to enhance ultrastructural contrast—scale bar: 100 nm [14].

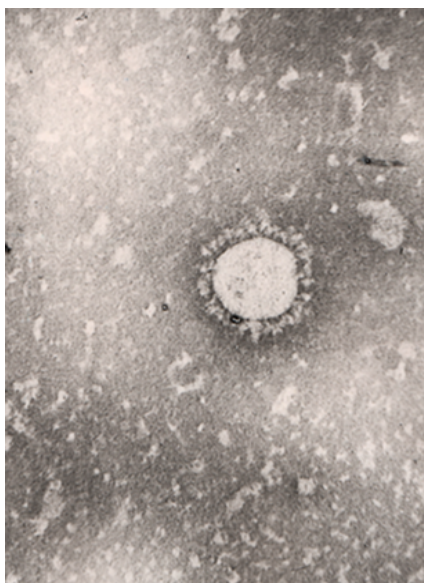


**Figure 8.** Transmission electron microscopy (TEM) image of an individual SARS-CoV-2 virion (B.1 lineage) isolated in Kazakhstan in 2021. The figure depicts a single, structurally intact virion visualised after propagation in Vero E6 cells at a multiplicity of infection (MOI) of 2. The

isolate, derived from a clinical specimen collected during the 2021 outbreak in Kazakhstan, is assigned to the B.1 lineage. The particle displays a spherical profile with a clearly defined corona-like outline generated by spike (S) glycoprotein projections. Its diameter is approximately 100 nm, consistent with the established ultrastructure of SARS-CoV-2. Negative staining enhances contrast of the viral envelope and surface spikes, confirming preservation of morphological integrity (scale bar: 100 nm) [14].

Recent advances in SARS-CoV-2 antiviral research provide a key mechanistic context for interpreting the synergistic interaction observed between Favipiravir and Ribavirin in this study. Broad reviews of COVID-19 pharmacotherapy emphasise that direct-acting antivirals targeting RNA-dependent RNA polymerase (RdRp), proteases, or spike-mediated entry remain the most mechanistically grounded treatment strategies, whereas agents lacking nucleotide- or polymerase-level activity—such as hydroxychloro-quine and chloroquine—have repeatedly failed to demonstrate virologic benefit in controlled trials [28-31]. Experimental work in Vero E6 and derivative cell systems further supports the use of polymerase-focused assays to evaluate nucleoside analogues: neutralisation and cytopathic-effect measurements have shown reproducible antiviral responses [32-34]. At the same time, ultrastructural studies confirm that the morphogenesis of SARS-CoV-2 in Vero E6 cells accurately reflects that of clinical isolates [33]. Moreover, systematic analysis of SARS-CoV-2 adaptation in Vero E6, VeroE6/TMPRSS2, and Calu-3 cells has revealed conserved replication features that maintain the relevance of poly-merase-targeting agents across viral lineages [34-35].

Host-directed pathways can also contribute to antiviral pressure. IL-33-stimulated group 2 innate lymphoid cells (ILC2s) demonstrate measurable suppression of viral persistence in pulmonary tissue [36], complementing the pharmacodynamic actions of nucleoside analogues that directly impair viral RNA synthesis. In contrast, studies of accessory proteins, such as the SIV Nef diacidic-motif mutant, illustrate how modulation of host-cell activation can influence viral replication without directly targeting the core replication machinery [37]. This distinction highlights why polymerase-directed drugs—including nucleoside analogues—exhibit more predictable antiviral outcomes across diverse viral contexts. These principles are reinforced by recent work in Kazakhstan, which demonstrates that Tenofovir exhibits targeted in vitro activity against the SARS-CoV-2 B.1 lineage and confirms conserved features within the NSP12 polymerase domain relevant to nucleotide-analogue susceptibility [35]. Complementary findings showing that an anti-HIV nucleotide analogue strongly inhibits SARS-CoV-2 in vitro and may offer benefit in long-COVID scenarios further underscore the translational value of polymerase-directed agents [14]. Together, these observations contextualise our findings and support the rationale for evaluating Favipiravir and Ribavirin as a dual-nucleoside

antiviral strategy, in which mutagenic pressure and GTP depletion act synergistically to limit SARS-CoV-2 replication.

## CONCLUSIONS

This study demonstrates that Favipiravir and Ribavirin exhibit a quantitatively synergistic antiviral interaction against SARS-CoV-2, with the most potent effect observed at a 1:1 ratio. CI, DRI, and isobologram analyses consistently showed that the combination outperforms additive expectations and enables meaningful dose reductions for both agents. The synergy reflects complementary mechanisms—Favipiravir-induced mutagenesis and Ribavirin-mediated GTP depletion—that together enhance pressure on the viral replication machinery despite SARS-CoV-2 proofreading capacity. Although full BSL-3 antiviral assays were not feasible, the combined cytotoxicity data, mechanistic evidence, and pharmacodynamic modelling provide a strong foundation for further preclinical evaluation. These findings support Favipiravir and Ribavirin as a rational dual-nucleoside strategy with potential applicability to SARS-CoV-2 and other RNA viruses requiring high-fidelity replication control.

A key limitation of this study is the absence of a complete live-virus antiviral assay per-formed under BSL-3 containment. Due to institutional restrictions during the research period, neither the Kazakhstan nor the China laboratories could provide sustained BSL-3 access for complete replication-competent SARS-CoV-2 experiments. To mitigate this constraint, we combined validated cytotoxicity assays (MTT and CCK-8), quantitative modelling, published antiviral benchmarks, and mechanistic alignment with established pathways for Favipiravir and Ribavirin. While these approaches provide strong predictive evidence of pharmacodynamic synergy, future work incorporating full viral titration assays and time-course inhibition studies under BSL-3 conditions will be essential to confirm the translational relevance of the observed drug–drug interaction.

Although the primary focus of project BR24992933 is the development of diagnostic models and therapeutic approaches for cancer patients, the funding framework encompasses broader molecular, cellular, and methodological research activities that strengthen national biomedical capacity. The experimental work conducted in this study—particularly the development of quantitative drug-interaction analyses, cytotoxicity assessment workflows, and cell-based evaluation platforms—directly contributes to these overarching goals by refining laboratory techniques applicable to oncology, virology, and therapeutic screening. The infrastructure, equipment access, and personnel support provided under this project enabled the generation, processing, and analysis of the datasets presented here. Thus, the study fits within the methodological and diagnostic-development components of BR24992933, even though its immediate scientific application relates to antiviral research.

In addition to the experimental findings, the rationale for evaluating synergistic antiviral combinations is supported by emerging clinical evidence demonstrating the systemic and immune-mediated consequences of SARS-CoV-2 infection and related antigenic stimulation. A recent case report described acute pancreatitis occurring shortly after administration of a vector-based COVID-19 vaccine, highlighting the ability of SARS-CoV-2-associated antigens to trigger dysregulated inflammatory responses beyond the respiratory tract [38]. Although causality cannot be inferred from isolated observations, such reports underscore the clinical importance of strategies to limit viral replication and secondary immune activation.

Furthermore, Guillain–Barré syndrome has been reported in patients recovering from SARS-CoV-2 pneumonia, particularly in immunocompromised settings, supporting the concept that sustained viral burden and post-infectious immune dysregulation may contribute to severe neurological complications [39, 40, 41, 42]. Collectively, these observations provide clinical justification for exploring synergistic antiviral regimens, such as the combination of Favipiravir and Ribavirin, which may achieve more effective suppression of viral replication and potentially reduce the risk of downstream immune-mediated pathology.

Author Contributions: Conceptualisation, S.K. and B.N.; methodology, S.K., B.N.; software, S.K., A.M.; validation, S.K.; formal analysis, S.K., A.Y., A.M., V.A., S. K. (Saule Kariyeva); investigation, S.K., A.M.; writing—original draft, S.K., B.N., A.Y., A.M., V.A., S. K. (Saule Kariyeva); writing—review and editing, S.K.; visualisation, A.M., S.K. All authors have read and agreed to the published version of the manuscript

## Abbreviations

Abbreviation	Definition
bp	Base pairs
BSL-3	Biosafety Level 3
CC <sub>50</sub>	50% Cytotoxic concentration
CCK-8	Cell Counting Kit-8
cDNA	Complementary DNA
CI	Combination Index
DMSO	Dimethyl sulfoxide
DMEM	Dulbecco's Modified Eagle Medium
DRI	Dose-Reduction Index
EC <sub>50</sub>	50% Effective concentration
EPON	Epoxy resin for electron microscopy
Fa	Fraction affected
FBS	Fetal bovine serum
IC <sub>50</sub>	50% Inhibitory concentration
IMPDH	Inosine monophosphate dehydrogenase
MTT	3-(4,5-Dimethylthiazol-2-yl)-2,5-diphenyltetrazolium bromide
MOI	Multiplicity of infection
PBS	Phosphate-buffered saline

PCR	Polymerase chain reaction
PFU	Plaque-forming units
RdRp	RNA-dependent RNA polymerase
SARS-CoV-2	Severe Acute Respiratory Syndrome Coronavirus 2
SI	Selectivity index
TAF	Tenofovir alafenamide
TDF	Tenofovir disoproxil fumarate
TCID <sub>50</sub>	Tissue culture infectious dose 50%
TEM	Transmission electron microscopy

**Copyright:** All these pictures, tables, and graphs are original or from other references

**Institutional Review Board Statement:** Not applicable for studies not involving humans or ani-mals

**Informed Consent Statement:** Not applicable for studies not involving humans.

**Data Availability Statement:** The original data presented in the study are openly available at <https://biotechlink.org/index.php/journal/article/view/548> and <https://www.ncste.kz/ru/informacziya-pozavershennyim-nauchnyim-issledovaniyam>. <https://doi.org/10.1128/mra.01114-22>.

**Acknowledgements:** The authors express their gratitude to Shenzhen University for providing the opportunity to conduct experimental work through the Program for Graduate Students (International Academic Mobility Program 01.07-25.09.2024). The authors also thank the Research Institute for Biological Safety Problems (Gvardeyskiy, Kordai 080409, Kazakhstan) and the Kazakh Institute of Oncology and Radiology (KazIOR, Almaty 050022, Kazakhstan) for performing the duplicate cytotoxicity and viability tests in 2025.

Conflicts of Interest: No conflict of interest.

## REFERENCES

- Furuta Y, Gowen BB, Takahashi K, Shiraki K, Smee DF, Barnard DL. Favipiravir (T-705), a novel viral RNA polymerase inhibitor. *Antiviral research*. 2013 Nov 1;100(2):446-54. DOI: 10.1128/AAC.49.3.981-986.2005.
- Joshi S, Parkar J, Ansari A, Vora A, Talwar D, Tiwaskar M, Patil S, Barkate H. Role of favipiravir in the treatment of COVID-19. *International Journal of Infectious Diseases*. 2021 Jan 1;102:501-8. DOI: 10.1016/j.ijid.2020.10.069
- Driouich JS, Cochin M, Lingas G, Moureau G, Touret F, Petit PR, Piorkowski G, Barthelemy K, Laprie C, Coutard B, Guedj J. Favipiravir antiviral efficacy against SARS-CoV-2 in a hamster model. *Nature communications*. 2021 Mar 19;12(1):1735. DOI: 10.1038/s41467-021-21992-w
- Zhao L, Zhong W. Mechanism of action of favipiravir against SARS-CoV-2: Mutagenesis or chain termination?. *The Innovation*. 2021 Nov 28;2(4). DOI: 10.1016/j.xinn.2021.100165
- Leysen P, Balzarini J, De Clercq E, Neyts J. The predominant mechanism by which ribavirin exerts its antiviral activity in vitro against flaviviruses and paramyxoviruses is mediated by inhibition of IMP dehydrogenase. *Journal of virology*. 2005 Feb 1;79(3):1943-7. DOI: 10.1128/JVI.79.3.1943-1947.2005
- Unal MA, Bitirim CV, Summak GY, Bereketoglu S, Cevher Zeytin I, Besbinar O, Gurcan C, Aydos D, Goksoy E, Kocakaya E, Eran Z. Ribavirin shows antiviral activity against SARS-CoV-2 and downregulates the activity of TMPRSS2 and the expression of ACE2 in vitro. *Canadian journal of physiology and pharmacology*. 2021;99(5):449-60. DOI: 10.1139/cjpp-2020-0734
- Messina E, Danise A, Ferrari G, Andolina A, Chiurlo M, Razanacolona M, Barakat M, Israel RJ, Castagna A. Ribavirin aerosol in the treatment of SARS-CoV-2: A case series. *Infectious Diseases and Therapy*. 2021 Dec;10(4):2791-804. DOI: 10.1007/s40121-021-00493-9
- Somovilla P, García-Crespo C, Martínez-González B, Soria ME, de Ávila AI, Gallego I, Mínguez P, Durán-Pastor A, Ferrer-Orta C, Salar-Vidal L, Esteban-Muñoz M. Atypical mutational spectrum of SARS-CoV-2 replicating in the presence of ribavirin. *Antimicrobial Agents and Chemotherapy*. 2023 Jan 24;67(1):e01315-22. DOI: 10.1128/aac.01315-22
- Zhao L, Li S, Zhong W. Mechanism of action of small-molecule agents in ongoing clinical trials for SARS-CoV-2: a review. *Frontiers in Pharmacology*. 2022 Feb 25;13:840639. DOI: 10.3389/fphar.2022.840639
- Rommasi F, Nasiri MJ, Mirsaiedi M. Antiviral drugs proposed for COVID-19: action mechanism and pharmacological data. *European Review for Medical & Pharmacological Sciences*. 2021 Jun 1;25(11). DOI: 10.26355/eurrev\_202106\_26060
- Chou TC. Drug combination studies and their synergy quantification using the Chou-Talalay method. *Cancer research*. 2010 Jan 15;70(2):440-6. DOI: 10.1158/0008-5472.CAN-09-1947
- García-Crespo C, de Ávila AI, Gallego I, Soria ME, Durán-Pastor A, Somovilla P, Martínez-González B, Muñoz-Flores J, Mínguez P, Salar-Vidal L, Esteban-Muñoz M. Synergism between remdesivir and ribavirin leads to SARS-CoV-2 extinction in cell culture. *British journal of pharmacology*. 2024 Aug;181(15):2636-54. DOI: 10.1111/bph.16344
- Burashev Y, Usserbayev B, Kutumbetov L, Abduraimov Y, Kassenov M, Kerimbayev A, Myrzakhmetova B, Melisbek A, Shirinbekov M,

- Khaidarov S, Tulman ER. Coding complete genome sequence of the SARS-CoV-2 virus strain, variant B.1.1, sampled from Kazakhstan. *Microbiology Resource Announcements*. 2022 Dec 15;11(12):e01114-22. DOI: 10.1128/mra.01114-22.
14. Khaidarov S, Hejran AB, Moldakaryzova A, Izmailova S, Nurgaliyeva B, Beisenova A, Mustafaeva A, Nurzhanova K, Belova Y, Satbayeva E, Aidarov A. An Anti-HIV Drug Is Highly Effective Against SARS-CoV-2 In Vitro and Has Potential Benefit for Long COVID Treatment. *Viruses*. 2025 Aug 27;17(9):1170. DOI: 10.3390/v17091170
  15. Berridge MV, Herst PM, Tan AS. Tetrazolium dyes as tools in cell biology: new insights into their cellular reduction. *Biotechnology annual review*. 2005 Jan 1;11:127-52. DOI: 10.1016/S1387-2656(05)11004-7.
  16. Tominaga H, Ishiyama M, Ohseto F, Sasamoto K, Hamamoto T, Suzuki K, Watanabe M. A water-soluble tetrazolium salt useful for colorimetric cell viability assay. *Analytical Communications*. 1999 Jan 1;36(2):47-50. DOI: 10.1039/A809656B
  17. Chaves OA, Sacramento CQ, Ferreira AC, Mattos M, Fintelman-Rodrigues N, Temerozo JR, Vazquez L, Pinto DP, da Silveira GP, da Fonseca LB, Pereira HM. Atazanavir is a competitive inhibitor of SARS-CoV-2 Mpro, impairing variants replication in vitro and in vivo. *Pharmaceuticals*. 2021 Dec 24;15(1):21. <https://doi.org/10.3390/ph15010021>.
  18. Ouyang W, Yu Z, Zhao X, Lu S, Wang Z. Aptamers in hematological malignancies and their potential therapeutic implications. *Critical Reviews in Oncology/Hematology*. 2016 Oct 1;106:108-17. <https://doi.org/10.1016/j.critrevonc.2016.08.003>.
  19. World Health Organization (WHO). Available online: <https://www.who.int/publications/i/item/who-whe-epp-2024.3>: 01 November 2025.
  20. De Clercq E, Li G. Approved antiviral drugs over the past 50 years. *Clinical microbiology reviews*. 2016 Jul;29(3):695-747. DOI: 10.1128/CMR.00102-15.
  21. Somovilla P, García-Crespo C, Martínez-González B, Soria ME, de Ávila AI, Gallego I, Mínguez P, Durán-Pastor A, Ferrer-Orta C, Salar-Vidal L, Esteban-Muñoz M. Atypical mutational spectrum of SARS-CoV-2 replicating in the presence of ribavirin. *Antimicrobial Agents and Chemotherapy*. 2023 Jan 24;67(1):e01315-22. DOI: 10.1128/aac.01315-22
  22. Driouich JS, Cochin M, Lingas G, Moureau G, Touret F, Petit PR, Piorkowski G, Barthelemy K, Laprie C, Coutard B, Guedj J. Favipiravir antiviral efficacy against SARS-CoV-2 in a hamster model. *Nature communications*. 2021 Mar 19;12(1):1735. DOI: 10.1038/s41467-021-21992-w
  23. Chen B, Julg B, Mohandas S, Bradfute SB. Viral persistence, reactivation, and mechanisms of long COVID. *Elife*. 2023 May 4;12:e86015. DOI: 10.7554/eLife.86015.
  24. Crotty S, Cameron C, Andino R. Ribavirin's antiviral mechanism of action: lethal mutagenesis?. *Journal of molecular medicine*. 2002 Feb;80(2):86-95. DOI: 10.1007/s00109-001-0308-0
  25. Chatterjee S, Bhattacharya M, Dhama K, Lee SS, Chakraborty C. Molnupiravir's mechanism of action drives "error catastrophe" in SARS-CoV-2: A therapeutic strategy that leads to lethal mutagenesis of the virus. *Molecular Therapy Nucleic Acids*. 2023 Sep 12;33:49-52. DOI: 10.1016/j.omtn.2023.06.006.
  26. Wang X, Sacramento CQ, Jockusch S, Chaves OA, Tao C, Fintelman-Rodrigues N, Chien M, Temerozo JR, Li X, Kumar S, Xie W. Combination of antiviral drugs inhibits SARS-CoV-2 polymerase and exonuclease and demonstrates COVID-19 therapeutic potential in viral cell culture. *Communications biology*. 2022 Feb 22;5(1):154. DOI: 10.1038/s42003-022-03101-9
  27. Good SS, Westover J, Jung KH, Zhou XJ, Moussa A, La Colla P, Collu G, Canard B, Sommadossi JP. AT-527, a double prodrug of a guanosine nucleotide analog, is a potent inhibitor of SARS-CoV-2 in vitro and a promising oral antiviral for treatment of COVID-19. *Antimicrobial Agents and Chemotherapy*. 2021 Mar 18;65(4):10-128. DOI: 10.1128/AAC.02479-20
  28. Huang J, Song W, Huang H, Sun Q. Pharmacological therapeutics targeting RNA-dependent RNA polymerase, proteinase and spike protein: from mechanistic studies to clinical trials for COVID-19. *Journal of clinical medicine*. 2020 Apr 15;9(4):1131. DOI: 10.3390/jcm9041131.
  29. McFee RB. COVID-19: Therapeutics and interventions currently under consideration. *Disease-a-Month*. 2020 Sep 1;66(9):101058. DOI: 10.1016/j.disamonth.2020.101058
  30. Sanders JM, Monogue ML, Jodlowski TZ, Cutrell JB. Pharmacologic treatments for coronavirus disease 2019 (COVID-19): a review. *Jama*. 2020 May 12;323(18):1824-36. DOI: 10.1001/jama.2020.6019.
  31. Wu Y, Li C, Xia S, Tian X, Kong Y, Wang Z, Gu C, Zhang R, Tu C, Xie Y, Yang Z. Identification of human single-domain antibodies against SARS-CoV-2. *Cell host & microbe*. 2020 Jun 10;27(6):891-8. DOI: 10.1016/j.chom.2020.04.023.
  32. Barreto-Vieira DF, da Silva MA, Garcia CC, Miranda MD, Matos AD, Caetano BC, Resende PC, Motta FC, Siqueira MM, Girard-Dias W, Archanjo BS. Morphology and morphogenesis of SARS-CoV-2 in Vero-E6 cells. *Memórias do Instituto Oswaldo Cruz*. 2021 Feb 8;116:e200443. DOI: 10.1590/0074-02760200443.

33. Kinoshita H, Yamamoto T, Kuroda Y, Inoue Y, Miyazaki K, Ohmagari N, Tokita D, Nguyen PH, Yamada S, Harada S, Kanno T. Improved efficacy of SARS-CoV-2 isolation from COVID-19 clinical specimens using VeroE6 cells overexpressing TMPRSS2 and human ACE2. *Scientific reports*. 2024 Oct 22;14(1):24858. DOI: 10.1038/s41598-024-75038-4
34. Aiewsakun P, Phumiphanjarpak W, Ludowyke N, Purwono PB, Manopwisedjaroen S, Srisaowakarn C, Ekronarongchai S, Suksatu A, Yuvaniyama J, Thitithanyanont A. Systematic exploration of SARS-CoV-2 adaptation to Vero E6, Vero E6/TMPRSS2, and Calu-3 cells. *Genome Biology and Evolution*. 2023 Apr 1;15(4):evad035. DOI: 10.1093/gbe/evad035.
35. Khaidarov S, Burashev Y, Kozhabergenov N, Usserbayev B, Melisbek A, Shirinbekov M, Moldakaryzova A, Beisenova A, Mustafaeva A, Kydyrbaeva A. Targeted in vitro-confirmation of the antiviral activity of Tenvir (Tenofovir) drug against the SARS-COV-2 virus variant B. in Kazakhstan and identifying NSP12 in the viral genome. *Eurasian Journal of Applied Biotechnology*. 2024 Jul 5(2):49-60. <https://doi.org/10.11134/btp.2.2024.6>.
36. Khaidarov S. Antiviral II-33-Stimulated Group 2 Innate Lymphoid Cells (Cd-90 And Cd-117) From Mouse Lungs. *Eurasian Journal of Applied Biotechnology*. 2024 Dec 3(4):84-90. <https://doi.org/10.11134/btp.4.2024.8>.
37. Tschulena U, Sanzenbacher R, Mühlebach MD, Berger A, Münch J, Schindler M, Kirchhoff F, Plesker R, Coulibaly C, Panitz S, Prüfer S. Mutation of a diacidic motif in SIV-PBj Nef impairs T-cell activation and enteropathic disease. *Retrovirology*. 2011 Mar 2;8(1):14. DOI: 10.1186/1742-4690-8-14
38. Nurgaliyeva B, Moldakaryzova A, Khaidarov S, Aldasheva Z. Acute pancreatitis as a rare adverse event following COVID-19 vector-based vaccination: A case report. *Acta Biomed*. 2025, 96, 17277. <https://doi.org/10.23750/abm.v96i6.17277>.
39. Nurgaliyeva B, Otunbayeva Z, Kan O, Moldakaryzova A, Khaidarov S, Izmailova Sand S, Abyldayeva G. Guillain-Barré Syndrome Following SARS-CoV-2 Pneumonia in a Patient Receiving Adjuvant Chemotherapy for Gastric Cancer: A Case Report. *International Tinnitus Journal*. 2025;29(2):85-90. <https://doi.org/10.5935/0946-5448.2025013>.
40. Alaagib, S. B., Alamri, Y., Alhashim, J., & Alduwais, A. A. M. (2025). The ecological footprint of AI: Informing sustainable development in agriculture. *Journal of Experimental Biology and Agricultural Sciences*, 13(4), 554–563. [https://doi.org/10.18006/2025.13\(4\).554.563](https://doi.org/10.18006/2025.13(4).554.563)
41. Koike, T., Yamamoto, S., Furui, T., Miyazaki, C., Ishikawa, H., & Morishige, K. I. (2023). Evaluation of the relationship between equol production and the risk of locomotive syndrome in very elderly women. *International Journal of Probiotics and Prebiotics*, 18(1), 7–13. <https://doi.org/10.37290/ijpp2641-7197.18:7-13>
42. Wang, D., Zhong, J., Gao, Y., He, J., Hou, J., & Du, K. (2024). Green tea extract improves postoperative outcomes after urological surgery. *Current Topics in Nutraceutical Research*, 22(3), 974–979. <https://doi.org/10.37290/ctnr2641-452X.22:974-979>